Using Magnetic Levitation for Non-Destructive Quality Control of Plastic Parts

Using Magnetic Levitation for Non-Destructive Quality Control of Plastic Parts

Jonathan W. Hennek[1], Alex Nemiroski[1], Anand Bala Subramaniam[1], David K. Bwambok[1], Dian Yang[2], Daniel V. Harburg[1], Simon Tricard[1], Audrey K. Ellerbee[1], and George M. Whitesides[1,3,4,*]

[1]Department of Chemistry and Chemical Biology, Harvard University,
12 Oxford St., Cambridge, MA 02138

[2]School of Engineering and Applied Sciences, Harvard University, 29 Oxford St., Cambridge, MA 02138

[3]Wyss Institute for Biologically Inspired Engineering, Harvard University,
60 Oxford St., Cambridge, MA 02138

[4]Kavli Institute for Bionano Science & Technology, Harvard University, 29 Oxford Street
Cambridge, MA 02138

* Corresponding author: George M. Whitesides (gwhitesides@gmwgroup.harvard.edu)

INTRODUCTION

Large-scale, reliable, and economical manufacturing of plastic objects ("parts")[1] is critical for a range of industrial applications (e.g. medical devices, automotive parts, small consumer goods, micro-electro-mechanical systems (MEMS), and optical devices, among others). Plastic parts are chosen (over metal, for example) in many cases, in order to lower the cost (as well as weight, corrosion resistance, and other properties) of the final assembled product. Depending on the scale of manufacturing, costs favor relatively simple techniques such as injection molding, casting, stamping, or machining for producing products with a range of shapes from raw, polymeric plastics.[1] Low-cost plastic parts must maintain an acceptable level of quality to avoid failure in use. In an optimized production process, occasional defects, such as voids, cracks, or embedded impurities can occur during routine manufacturing.[2–7] Defective parts, if not identified, can lead to the failure of the final assembled product. Non-destructive methods are thus required to identify defective parts that deviate from quality standards resulting either from manufacturing (both process optimization and volume production) or improper storage or use of the part.

Current non-destructive methods that have been used to test the quality of molded parts in specialized and critical applications include industrial computed tomography (ICT),[8,9] infrared thermography,[10] and ultrasonic testing.[11] The cost and complexity associated with the use of these instruments often prevent their application in routine quality control and, therefore, during the development and use of a manufacturing process, visual inspection may be the only form of quality control. In this paper, we demonstrate how magnetic levitation (MagLev) enables (i) the identification of parts with embedded defects, (ii) the separation of a defective part from a single batch, (iii) the characterization of certain kinds of defects, and (iv) the detection of counterfeit, high-value plastic parts. MagLev can suspend and orient[12] an object without contact by balancing gravitational and magnetic forces.[13] Here we show that the orientation of a part that is

magnetically levitated depends strongly on both its shape and heterogeneity in density. This characteristic enables rapid identification of a defective part by visual inspection of the levitation height or angle of orientation in comparison to the rest of the parts in the batch. The method is inexpensive, non-destructive and straightforward to implement. The portability of the MagLev device has the potential to allow quality control of parts at the point-of-manufacturing, the point-of-sale, and the point-of-use.

We used a similar MagLev device setup to those previously described.[13] Briefly, the object is suspended in a container filled with a paramagnetic solution (e.g., aqueous manganese chloride, $MnCl_2$, or paramagnetic ionic liquids)[14] and the container is placed between two NdFeB magnets oriented with like poles facing each other (Figure 1). In this configuration of the magnets, the magnetic gradient along the vertical centerline is approximately linear, and the vertical equilibrium position of the diamagnetic object within the device — its levitation height, h, measured as the distance between the face of the bottom magnet to the centroid of the object— correlates linearly with its volume-averaged density $\overline{\rho}_s$ (kg/m^3), as shown in Equation 1.[13]

$$h = \frac{(\overline{\rho}_s - \rho_m) g \mu_o d^2}{(\overline{\chi}_s - \chi_m) 4 {B_0}^2} + \frac{d}{2} \qquad (1)$$

In this equation, ρ_m (kg/m^3) is the density of the paramagnetic medium, $\overline{\chi}_s$ is the volume-averaged magnetic susceptibility of the sample (SI, unitless), χ_m is the magnetic susceptibility of the medium (SI, unitless), d (m) is the distance between the magnets, B_0 (Tesla) is the magnitude of the magnetic field at the surface of the magnets, g (m/s^2) is the acceleration due to gravity, and μ_o (T·m·A^{-1}) is the magnetic permeability of free space.

We and others have used MagLev to classify forensic evidence,[15] analyze biological systems,[16,17] determine the quality of food,[18] separate crystal polymorphs,[19] separate enantiomers and racemates,[20] and determine the environment used for self-assembly,[21] among

other applications.[22–31] Recently, we used MagLev to orient and assemble objects in three dimensions without mechanical contact.[12] We showed that objects of homogenous density, but of anisotropic shape, oriented with their long axis parallel or perpendicular to the surface of the magnets in a manner that depended on their aspect ratio.[12] The analytical model developed in that work suggested that objects with regions of heterogeneous density should deviate from this behavior. We thus hypothesized that observing the orientation that a part adopts in a MagLev device might be a means to detect defects in plastic parts.

To test this hypothesis, we selected a commercial batch of plastic parts consisting of 23 Nylon 6 washers purchased from McMaster-Carr. All the washers appeared undamaged and free from defects by visual inspection (although they were opaque). We levitated each of the washers sequentially in a solution of 0.10 M $MnCl_2$ + 1.26 M $ZnCl_2$ and measured α, the angle that the washer oriented with respect to the surface of the magnets. We plotted a histogram of the values of α in Figure 2A. Most of the washers levitated with α = 0-16°; this narrow distribution indicated that the washers were relatively homogeneous. This observation is expected since the washers were produced using an optimized process. One washer deviated significantly, however, and levitated at α = 45° (Figure 2B).

Figure 1. A schematic of the MagLev device used in this work. Plastic parts to be analyzed are placed within a container of paramagnetic medium and levitate at a height, *h*, above the surface of the bottom magnet where the gravitational and magnetic forces balance. We define the laboratory frame of reference with coordinates (x,y,z) and the body-fixed, principal frame of reference with coordinates (u,v,w). For an object with heterogeneity in density, the orientation of the object can be measured as an angle θ between the w- and z- axes or as an angle α between the w- and y- axes.

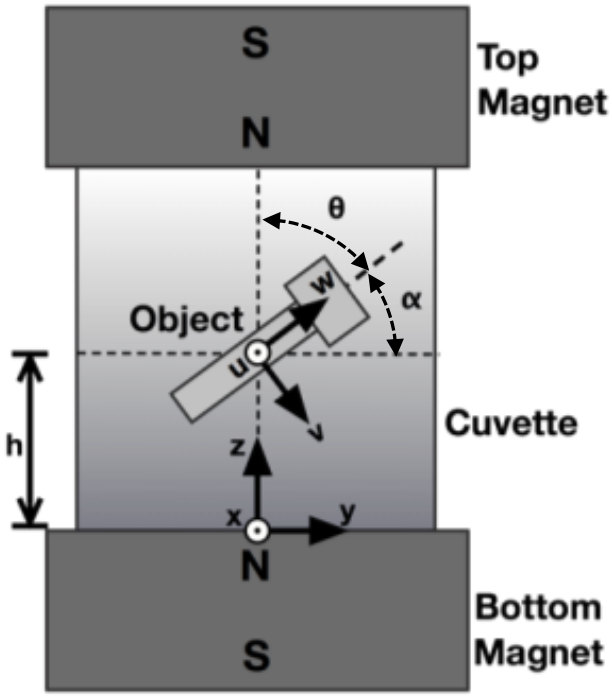

Since each of these washers appeared visually indistinguishable, we reasoned that an internal defect could have led to the observed deviation in α. We thus performed micro-computed tomography (micro-CT) on the washer that was an outlier ($\alpha = 45°$) and two "normal" washers with α of 3° and 10°. Micro-CT, a form of industrial computed tomography (ICT), employs x-rays to obtain two-dimensional cross-sections that can be stitched together to form a three-dimensional rendering of the internal structure of an object. Figure 2 (panels E-G) shows the micro-CT images with detected inclusions (purple) and pores (green) (see Supporting Information for details). The washer with $\alpha = 3°$ was found to have ~50 small pores distributed relatively symmetrically with some local concentration near the inner edge of the washer. The volume of these pores ranged from 1.1 to 5.2 x 10^{-4} mm^3; the volume of the washer is 198 mm^3. Molded Nylon 6 is known to be a slightly porous material.[3] The washer with $\alpha = 10°$ was observed to have ~300 similarly sized pores concentrated symmetrically on the inner edge and asymmetrically on the outer edge of the washer. The washer that levitated with $\alpha = 45°$ was found to have an inclusion defect with a volume of 0.014 mm^3 (Figure 2G inset), significantly larger than the volume of the pores. The greater x-ray contrast of this region suggests that this defective region had a higher density than the surrounding Nylon 6.

Notably, the MagLev technique was able to detect the presence of this defect in an opaque washer using a tabletop configuration of magnets in less than 2 s. In contrast, the micro-CT required ~2 hours per scan and several additional hours of computation and data analysis. Although micro-CT provides high-resolution information of the shape and location of the defect, such information may not be necessary for most quality control applications. Micro-CT, in addition, is only available in well-equipped facilities, requires skilled operators, and costs several hundred thousand dollars. MagLev can be used to infer that the inclusion defect was of higher density than the surrounding polymer because that region was closer to the bottom magnet.

MagLev thus provides a simple, inexpensive means of determining the presence of inclusion defects in plastic parts.

We previously reported that objects of anisotropic shape, but homogeneous density, levitate in the device with its center of volume (centroid) located in the central axis of the MagLev device and orients so that it occupies the least amount of volume in regions of high magnetic field strength.[12] The controlling parameters are the lengths of the principal axes of the object, $(\lambda_u, \lambda_v, \lambda_w)$, which are geometric parameters that reflect how points within the object are distributed with regard to an arbitrary axis in the body-fixed frame of reference. For objects with regions of inhomogeneous density, for example objects with defects, the effect of the distribution of mass on the orientation has to also be considered. To quantify the ability of the MagLev for identifying defects, we extend this model here to also include the orientation of objects with an arbitrary distribution of density in MagLev. Equation 2 describes the potential energy U for an arbitrary object in a magnetic field, where $\Delta\chi = \overline{\chi}_s - \chi_m$, $\Delta\rho = \overline{\rho}_s - \rho_m$, $\mathbf{B} = \mathbf{B}(\mathbf{r})$ is the magnetic field, $\mathbf{r}_{cm} = (u_{cm}, v_{cm}, w_{cm})$ is the center of mass of the object (relative to its centroid) in the MagLev frame of reference, $\hat{\mathbf{z}}$ is the unit vector of the z-axis, and V is the volume of the object. The primed coordinates indicate the frame of reference that is fixed with the orientation of the object (body-fixed frame of reference).

$$U = U_{mag} + U_{grav}$$

$$= -\int_V \left(\frac{\Delta\chi}{2\mu_o}\mathbf{B}\cdot\mathbf{B} + \Delta\rho g\mathbf{r}_{cm}\cdot\hat{\mathbf{z}}\right)dV. \qquad (2)$$

In general, for a diamagnetic object in a paramagnetic medium, $\Delta\chi < 0$. Equation 3 gives the energy of orientation of the object in the Maglev (See SI for full derivation and details). The second term in Equation 3 accounts for the gravitational torque on the object due to the asymmetric distribution of mass ($r_{cm} \neq 0$) within the object.

$$U(\theta,\phi) = -\frac{2{B_0}^2 \Delta\chi V}{\mu_o d^2}\left[{\lambda_v}^2 - {\lambda_w}^2 + \left({\lambda_u}^2 - {\lambda_v}^2\right)\sin^2\phi\right]\sin^2\theta$$
$$- \overline{\rho}_s V g(u_{cm}\sin\theta\sin\phi + v_{cm}\sin\theta\cos\phi + w_{cm}\cos\theta). \quad (3)$$

In this equation, we have assumed the magnetic field is linear ($\mathbf{B} = \frac{2B_0}{d} z\,\hat{\mathbf{z}}$) and that $\Delta\chi$ is homogenous throughout the volume V of the object. Inspecting the first term (magnetic contribution), we see that, in general, the principal axes λ_l are determined by ${\lambda_l}^2 = \frac{1}{V}\int_V l^2 dV$, and will compete to determine the preferred orientation of the object in the magnetic field; for $r_{cm} = 0$, the second term in Equation 3 is zero and the largest λ_l will always orient perpendicular to the z-axis. If $r_{cm} \neq 0$, there will be an additional torque about the centroid that acts to tilt the object and move the center-of-mass downwards. Just as the gravitational and magnetic forces balance at the equilibrium height of the object, the gravitational and magnetic torques balance at the equilibrium orientation—the equilibrium angle of orientation (θ, ϕ) will occur where U is minimized. We have ignored terms that depend on h because they do not couple to the angular orientation (SI).

We first consider the simple case of a rod with density ρ_r, length L, and square cross-section with side-length W. Because we are free to choose the starting orientation of the principal axes with respect to the MagLev reference frame, we chose a starting orientation of the rod such that the degenerate principal axes are $\lambda_u = \lambda_v$, and thus, for W along $\hat{\mathbf{u}}$ and $\hat{\mathbf{v}}$ and L along $\hat{\mathbf{w}}$, we have ${\lambda_u}^2 = {\lambda_v}^2 = W^2/12$ and ${\lambda_w}^2 = L^2/12$. If we now insert a small cubic inclusion with density ρ_i, volume V_i, and displacement z_i along the w-axis, then U simplifies to Equation 4.

$$U(\theta) = -\frac{{B_0}^2\Delta\chi}{6\mu_o d^2} V(W^2 - L^2)\sin^2\theta + (\rho_i - \rho_r)V_i z_i \cos\theta \quad (4)$$

The magnetic contribution (first term) to the equilibrium orientation of the rod is completely determined by the competition between W and L: (i) for $L < W$ (short rod), the w-axis will orient

towards $\theta_0 = 0^\circ$ or 180° (L along z-axis) and (ii) for $L > W$ (long rod), the w-axis will orient towards $\theta_0 = 90^\circ$ or 270° (L along y-axis). In the first case, the gravitational torque is always zero. In the second case, if $V_i z_i \neq 0$, the final equilibrium angle will be $\theta = \theta_0 + \alpha$, where α is the angular deviation from magnetic equilibrium caused by a non-zero gravitational torque. In general, the side of the object with the defect will tip down if $\rho_i > \rho_r$ and will tip up if $\rho_i < \rho_r$. Larger values of V_i, $(\rho_i - \rho_r)$, or z_i will lead to larger values of θ. The rod-shaped geometry lends itself to relatively simple analytical treatment; more complicated geometries and configuration of defects can be analyzed by numerically solving Equation 3.

To test our predictions experimentally, we used a 3D printer capable of printing materials with dissimilar densities to create model objects (see SI for details). We made rods (L = 2.5 cm and W = 1.0 cm) out of polyacrylate (ρ_r = 1.184 g/cm^3) that incorporated a series of less dense inclusions of the same material, but with a lesser degree of crosslinking and a lower density (ρ_i = 1.163 g/cm^3). The rods were fabricated with different inclusion volumes V_i and inclusion locations z_i (as measured from the centroid of the rod). Seven rods of each type were levitated in 0.05 M $MnCl_2$ in a MagLev device with rectangular prism magnets (2.5 x 2.5 x 10 cm, magnetized through the 2.5 x 10 cm face) used to confine the rods to the y-z plane (discussed in the SI) and α was recorded. We determined $B_0 = 0.385$ T with a magnetometer (AlphaLab Inc.) and assumed $\bar{\chi}_s = 0.58 \times 10^{-5}$.[32] To determine χ_m at room temperature (296 K), we used the standard relation $\chi_m = 1.85811 \times 10^{-4}[MnCl_2] - 9 \times 10^{-6}$, described by Mirica *et al.*[13]

Measurements (squares with error bars) and modeled values (solid line) are shown in Figure 3. As the V_i at a fixed $z_i$increases, from 6.6 mm^3 to 52.7 mm^3, so does α (Figure 3A). Note that the pristine rod levitates at a small non-zero angle, most likely due to small non-uniformity in the cross-linking of polyacrylate. The volume fraction of an inclusion (VF), that is, the percentage of the total rod volume encompassed by the inclusion, is shown as an additional x-axis in Figure

3A. When the location is changed of an inclusion of a given volume (VF = 0.63%), α changes (Figure 3B); as the inclusion moves closer to the centroid of the rod, α decreased. Also shown (as an open square) is the levitation angle of a rod with two identical inclusions on opposing ends of the rod. One limitation of MagLev is that it is unable to detect a deviation from horizontal if the defects in an object are exactly symmetrical (or in the exact center of the object), which is difficult to obtain except by design. If the difference in density due to the added inclusions was sufficiently large, however, the rods would levitate at a different height since the average density would be changed.

We quantified the sensitivity of MagLev as a method of detection for defects by selecting one type of rod/inclusion configuration (VF = 2.11%, z_i = 10 mm) and determining α for different concentrations of $MnCl_2$ (Figure 3C). As the concentration of the paramagnetic salt increased, α decreased. Thus, MagLev can be designed to detect defects within a certain tolerance by modifying the magnetic susceptibility of the medium.

We also used this analytical model to examine the effect on α of a single void (i.e., air pocket) of varying size in a 2.5-cm^3 rod. We found that, for a given MagLev setup (magnets = 2.5 x 2.5 x 10 cm^3, 4.5 cm apart), paramagnetic solution (0.05 M $MnCl_2$), and location of the void (z_i = 10 mm), even a small inclusion of 0.2 mm^3—only 0.008% of the total volume of the rod – would lead to a relatively large orientation angle (α > 10 °).

Figure 2. A) Histogram of a batch of Nylon 6 washers showing distribution in their levitation angle, α, measured horizontal to the face of the magnet, typically < 16° in 0.10 M $MnCl_2$ + 1.26 M $ZnCl_2$. The angle for one washer deviated significantly (α = 45°). Photographs show three washers levitating at ~3° (B), 10° (C), and 45° (D). The cross in the background is a visual reference. Images have been modified to increase contrast. E-G) Micro-CT images of the same washers showing similar porosity (green) in all and an inclusion (0.014 mm^3) with a greater density in the abnormal washer, leading to a different levitation height.

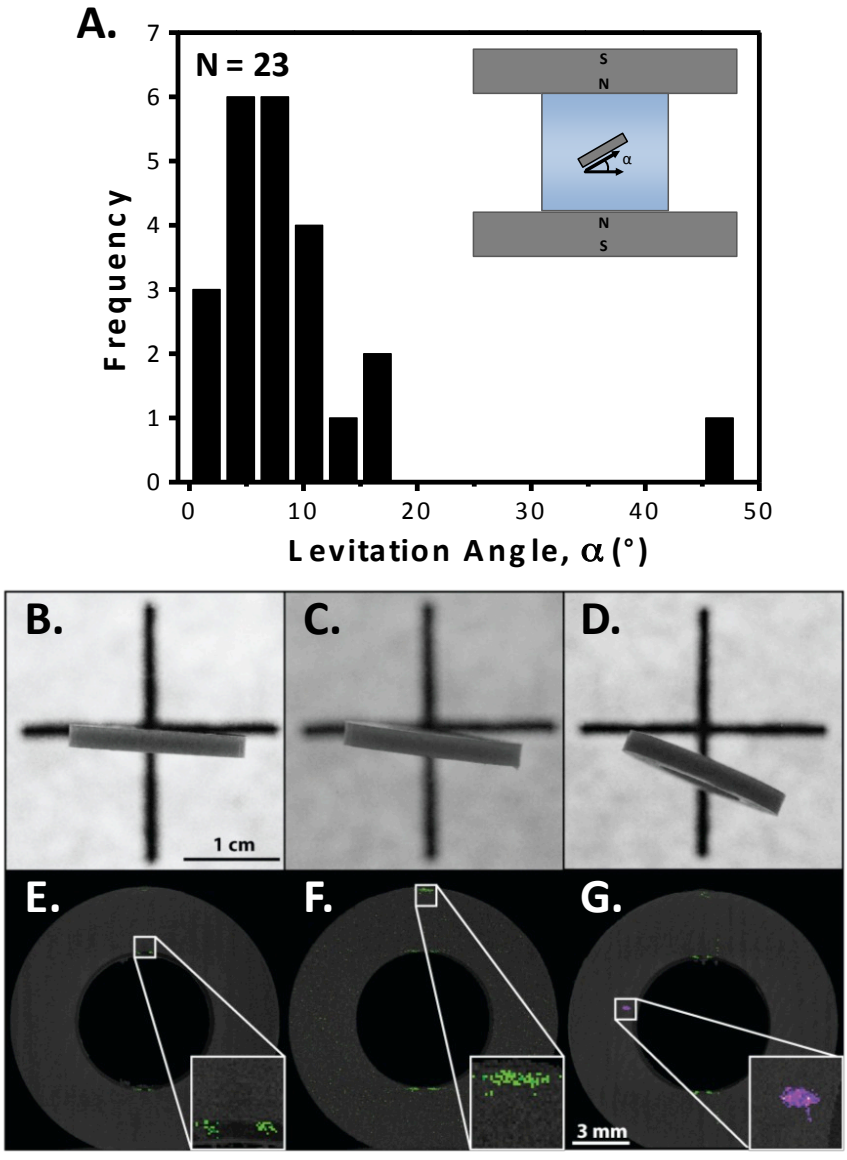

Figure 3. Levitation angle, α, for a variety of 3D-printed polyacrylate rods (ρ = 1.184 g/cm^3) containing inclusions of lower density polyacrylate (ρ = 1.163 g/cm^3) as a function of: A) inclusion volume, V_i, for a given location, z_i,, B) inclusion distance from the centroid of the rod, and C) $MnCl_2$ concentration for a given inclusion size and location. Experimental data are shown as squares (n = 7), and results of calculations are shown as a solid line.

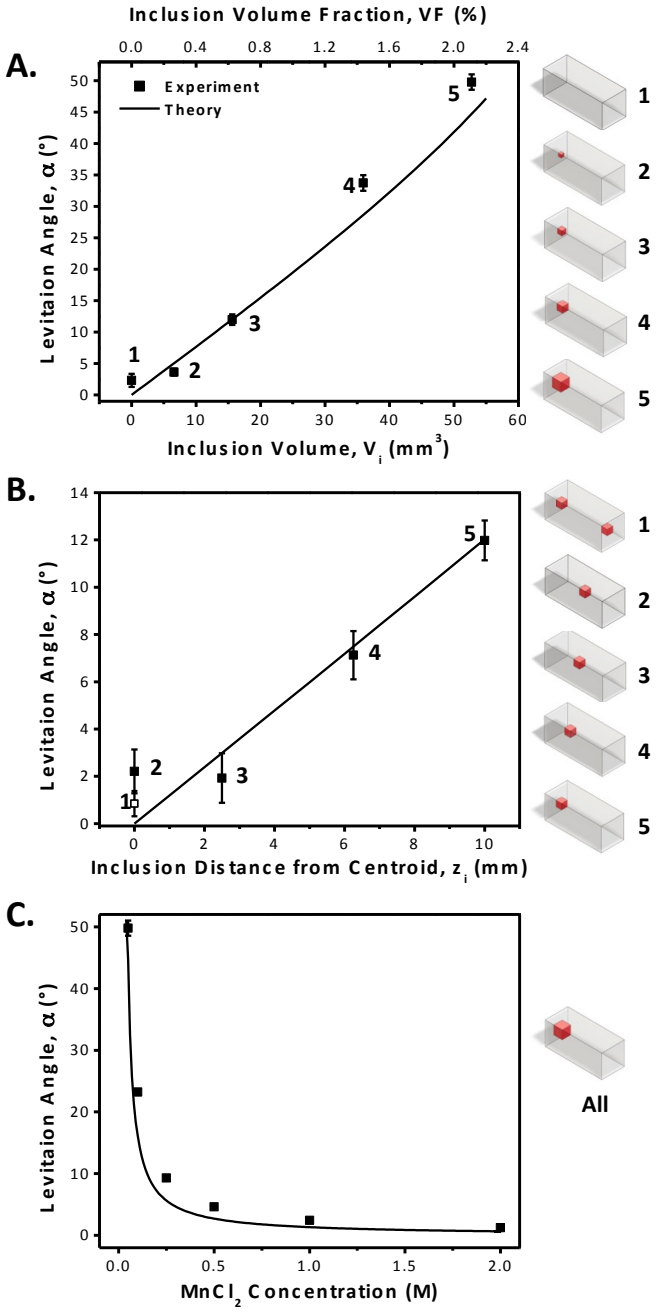

In addition to defects that arise during the manufacturing process, improper storage or use, or exposure to extreme environmental conditions, can lead to degradation of plastic parts that affects performance.[33] Plastics commonly undergo undesired changes in their properties upon exposure to a variety of environmental conditions (heat, moisture, UV-light, salt water, etc.).[3] Acids, salts, thermal stress and UV-light are known to cause chain scissioning in polymers, including Nylon.[34] Currently, there is no simple method to detect degradation of parts due to exposure to damaging environmental conditions or improper storage. We hypothesized that chain scissioning and subsequent rearrangement of the polymer chains and migration of the scissioned monomers and oligomers through the polymer (or out into the environment) could lead to a decrease in density that can be detected using MagLev.

We simulated conditions of improper storage or use (excessive sun exposure) of Nylon 6/6 parts. We placed 30 rods in a container and exposed them to UV-light for 36 hours (3.6 kW·h). A control set of pristine rods was stored in the dark to simulate proper storage in a warehouse or toolbox. After the prescribed exposure period, each rod was rinsed with DI water, placed into a solution of 0.10 M $MnCl_2$ + 1.26 M $ZnCl_2$ and levitated in a MagLev device. We measured α and plotted a histogram as shown in Figure 4. Pristine rods levitated with a clustered distribution of $\alpha < 3°$. The UV-light exposed rods, on the other hand, exhibited a large variation in α; the exposure caused a non-uniform change in density in many of the parts. In the container, some of the rods were entirely exposed to the UV light while others were only exposed over a small area due to the jumbled arrangement of the rods (see inset of Figure 4).

To further understand these observations, we chose seven rods, exposed half of each rod to UV light (100 W), and measured the angle of the rods at 12-hour intervals for 72 hours. Figure S3 shows α of the rods versus illumination time. The regions exposed to light show a reduction in density as evidenced by the positive α (measured as the exposed half above horizontal); we

confirmed that the exposed region was responsible for the net decrease in density. The SI shows the behavior of rods subjected to other harsh environmental conditions, such as 50 °C deionized water, sea water (0.60 M NaCl), a solution of acid (0.10 M HCl), and localized thermal stresses (Figure S4-S5).

In addition to detecting defective parts, MagLev can be used to identify counterfeit parts that differ in density from genuine high-quality plastics. During the fabrication of high-value plastics, manufacturers (and counterfeiters) must control for molecular weight, crystallinity, porosity, and composition of additives.[35] Deviation from a controlled process for any of these parameters can alter the density of the material. Counterfeiting of high-value plastic parts is a serious challenge for the plastics industry and global trade regulators. In the absence of accepted industry standards or universal recognition of patent/branding rights, customers are forced to trust suppliers or rely on expensive and time consuming testing methods to verify authenticity. For example, Tristar Plastics, the exclusive United States distributor of Rulon, a class of branded PTFE derivatives, recommends seven characterization methods to ensure parts meet standards and are authentic: dynamic mechanical analysis, thermomechanical analysis, thermogravimetric analysis, differential scanning calorimetry, Fourier transform infrared spectroscopy, scanning electron microscopy, and particle analysis.[35]

Figure 4. Histogram of the levitation angle, α, of A) pristine Nylon 6/6 rods or B) rods having been exposed to a 100 Watt UV-light for 36 hours (3.6 kW·h). For both cases N = 30 rods and the paramagnetic solution was 0.075 M $MnCl_2$ in water.

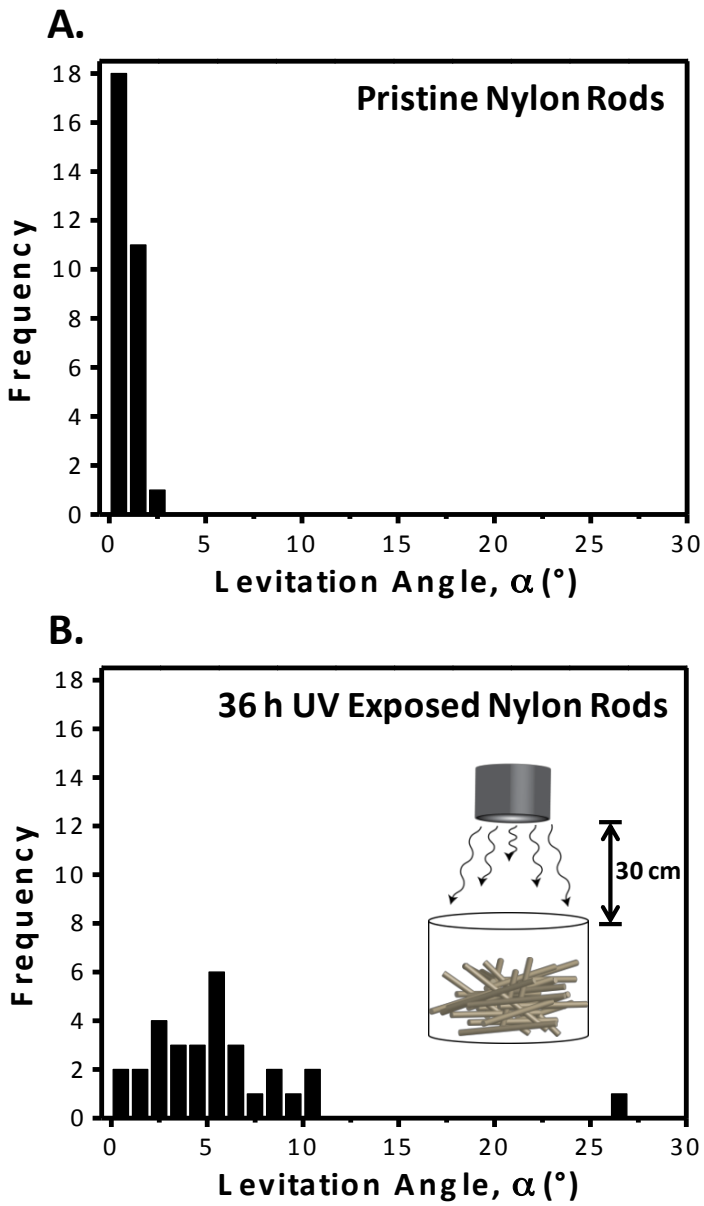

We obtained several types of real and fake Rulon® from Tristar Plastics. Rulon® bearings can cost several dollars per part (in comparison a Nylon washer which costs <$0.10) and, in the case of Rulon® 641, are FDA-approved for applications in the food industry, making them particularly attractive for counterfeiters. A search of the term "Rulon®" on Alibaba.com, the world's largest online commerce site that hosts listings from independent manufactures and suppliers, reveals 82 suppliers with products claiming to be genuine Rulon®. Fake Rulon® is manufactured to closely match the color of genuine Rulon®: fake and genuine Rulon® 641 are visually indistinguishable.

We simultaneously levitated real and fake Rulon® 641 in 0.40 M $MnCl_2$ in a 30% water, 70% Heavy Liquid (GEOLiquids Inc.; 2.242 g/cm^3) solution and recorded the height of each part. Figure 5 shows a box plot of the levitation height of seven real and fake bearings and a representative image of the bearings levitating in a MagLev device. A significant difference (p-value = 2.8 x 10^{-6}) in average height between real and fake Rulon® 641 was observed (h_{avg} = 2.80 ± 0.14 cm and 1.24 ± 0.09 cm, corresponding to calculated ρ_{avg} = 2.23 ± 0.01 and ρ_{avg} = 2.27 ± 0.01). We also tested Rulon® J, a derivative typically used for start-stop applications, and found that real and fake consistently levitate at different heights (Figure S6). We also found that trace quantities of magnetic material in Rulon® LR allowed us to use the detection of magnetic properties in MagLev as a further test of authenticity (see SI for more details).

Taken together, these results suggest that Maglev can be used to detect defects in plastic parts by monitoring the levitation angle or height of the parts. The method is particularly useful for exposing defects in opaque parts where visual inspection is impossible. The orientation of a prototype part in MagLev can thus be used as a simple and rapid means to detect voids, crystalline regions, or inclusions during the manufacturing process. At the consumer end, MagLev can be used to detect the occasional defective part that may have skipped the quality control process. Furthermore, MagLev can detect the presence of regions of degraded polymer due to exposure to

UV light and other harsh environments. In detecting counterfeit plastics, MagLev can save time and money at the point-of-sale by reducing the number of tests required to identify counterfeits (or increase the cost and complexity to counterfeiters by requiring density matching). If a batch of parts has a density significantly different than a verified authentic part, it can be assumed that the batch is not authentic and further testing is not necessary. We believe that along with plastic parts, measurement of heterogeneity in density using MagLev can be extended to detect defects in other materials, including fiber optic cables, ceramics, glass, fire-protecting tiles, among others.

Figure 5. A) Box plot showing levitation height for real and fake Rulon® 641 (n = 7) levitating at the same time. The significant difference in levitation height suggests a reproducible difference in density between real and fake Rulon®. B) Photograph of representative real and fake Rulon® 641 levitating in 0.40 M $MnCl_2$ in 30% water, 70% Heavy Liquid.

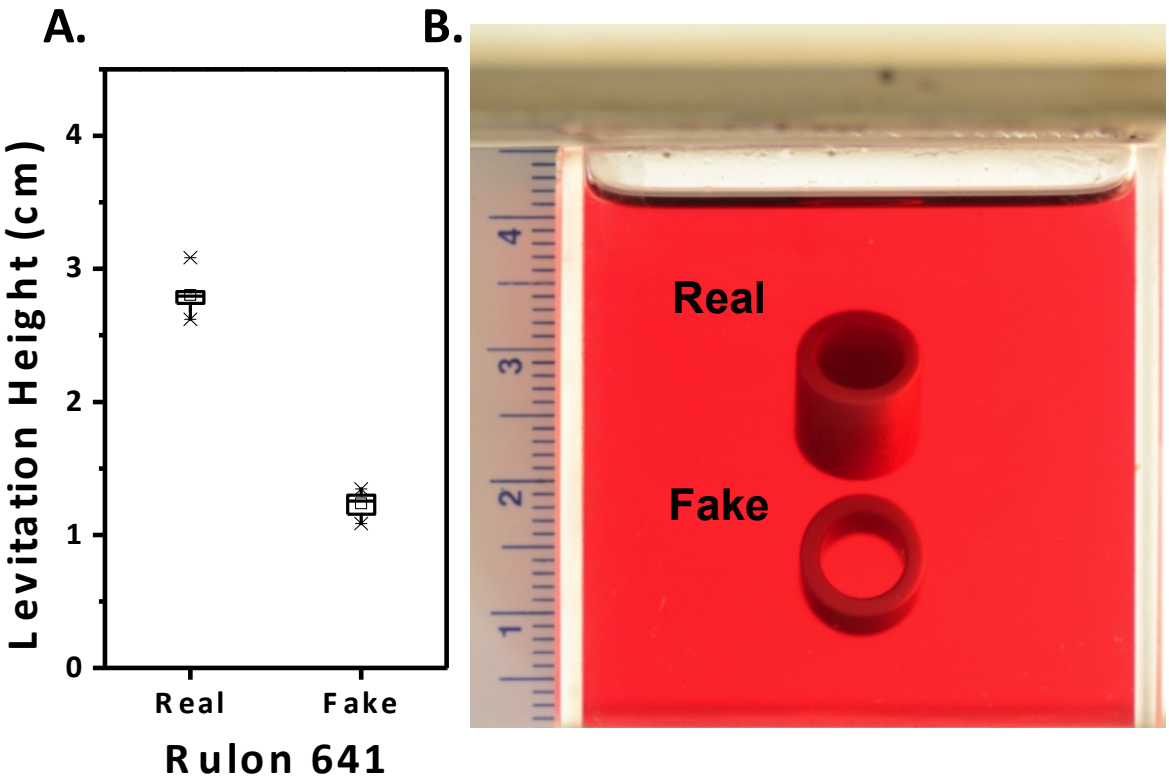

TOC GRAPHIC

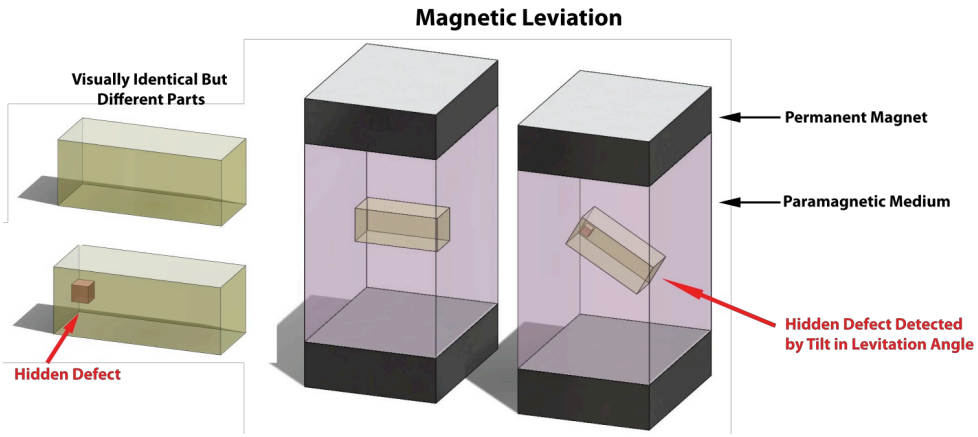

SUPPORTING INFORMATION

Supporting Information is available from the Wiley Online Library or from the authors.

ACKNOWLEDGEMENTS

This work was funded by Bill and Melinda Gates Foundation award #51308. D.Y. acknowledges the Wyss Institute for Biologically Inspired Engineering. A.K.E. acknowledges the Ford Foundation Postdoctoral Fellowship. We thank John Winzeler at Winzeler Gear and Dave Biering at TriStar Plastics for providing plastic parts, and for helpful discussions. This work was performed in part at the Center for Nanoscale Systems (CNS), a member of the National Nanotechnology Infrastructure Network (NNIN), which is supported by the National Science Foundation under NSF award no. ECS-0335765. CNS is part of Harvard University.

REFERENCES

[1] C. A. Harper, Ed., *Handbook of Plastics Technologies*, McGraw-Hill, **2006**.

[2] Z. Chen, L.-S. Turng, *Adv. Polym. Technol.* **2005**, *24*, 165.

[3] D. V. Rosato, D. V. Rosato, M. G. Rosato, *Injection Molding Handbook*, Kluwer Academic Publishers, **2000**.

[4] R. D. Adams, P. Cawley, *NDT Int.* **1988**, *21*, 208.

[5] V. Tvergaard, *Int. J. Fract.* **1982**, *18*, 237.

[6] R. M. McMeeking, *J. Mech. Phys. Solids* **1977**, *25*, 357.

[7] L. Xu, R. J. Crawford, *J. Mater. Sci.* **1993**, *28*, 2067.

[8] M. Bieberle, F. Barthel, H.-J. Menz, H.-G. Mayer, U. Hampel, *Appl. Phys. Lett.* **2011**, *98*, 34101.

[9] S. Persson, E. Östman, *Appl. Opt.* **1985**, *24*, 4095.

[10] Y. J. Song, W. Zhang, D. D. Wang, G. F. Jin, *Appl. Mech. Mater.* **2012**, *148*, 914.

[11] M. Kobayashi, *Int. J. Plast.* **1998**, *14*, 511.

[12] A. B. Subramaniam, D. Yang, H.-D. Yu, A. Nemiroski, S. Tricard, A. K. Ellerbee, S. Soh, G. M. Whitesides, *Proc. Natl. Acad. Sci. U. S. A.* **2014**, *111*, 12980.

[13] K. A. Mirica, S. S. Shevkoplyas, S. T. Phillips, M. Gupta, G. M. Whitesides, *J. Am. Chem. Soc.* **2009**, *131*, 10049.

[14] D. K. Bwambok, M. M. Thuo, M. B. J. Atkinson, K. A. Mirica, N. D. Shapiro, G. M. Whitesides, *Anal. Chem.* **2013**, *85*, 8442.

[15] M. R. Lockett, K. A. Mirica, C. R. Mace, R. D. Blackledge, G. M. Whitesides, *J. Forensic Sci.* **2013**, *58*, 40.

[16] N. D. Shapiro, K. A. Mirica, S. Soh, S. T. Phillips, O. Taran, C. R. Mace, S. S. Shevkoplyas, G. M. Whitesides, *J. Am. Chem. Soc.* **2012**, *134*, 5637.

[17] N. D. Shapiro, S. Soh, K. A. Mirica, G. M. Whitesides, *Anal. Chem.* **2012**, *84*, 6166.

[18] K. A. Mirica, S. T. Phillips, C. R. Mace, G. M. Whitesides, *J. Agric. Food Chem.* **2010**, *58*, 6565.

[19] M. B. J. Atkinson, D. K. Bwambok, J. Chen, P. D. Chopade, M. M. Thuo, C. R. Mace, K. A. Mirica, A. A. Kumar, A. S. Myerson, G. M. Whitesides, *Angew. Chemie Int. Ed.* **2013**, n/a.

[20] X. Yang, S. Y. Wong, D. K. Bwambok, M. B. J. Atkinson, X. Zhang, G. M. Whitesides, A. S. Myerson, *Chem. Commun. (Camb)*. **2014**, *50*, 7548.

[21] K. A. Mirica, F. Ilievski, A. K. Ellerbee, S. S. Shevkoplyas, G. M. Whitesides, *Adv. Mater.* **2011**, *23*, 4134.

[22] T. Kimura, *Polym. J.* **2003**, *35*, 823.

[23] T. Kimura, S. Mamada, M. Yamato, *Chem. Lett.* **2000**, 1294.

[24] A. T. Catherall, P. López-Alcaraz, K. A. Benedict, P. J. King, L. Eaves, *New J. Phys.* **2005**, *7*, 118.

[25] R. D. Waldron, *Rev. Sci. Instrum.* **1966**, *37*, 29.

[26] I. Simon, *Rev. Sci. Instrum.* **1968**, *39*, 1666.

[27] R. Evrard, *J. Vac. Sci. Technol.* **1969**, *6*, 279.

[28] K. Guevorkian, J. M. Valles, *Proc. Natl. Acad. Sci. U. S. A.* **2006**, *103*, 13051.

[29] Y. Ikezoe, T. Kaihatsu, S. Sakae, H. Uetake, N. Hirota, K. Kitazawa, *Energy Convers. Manag.* **2002**, *43*, 417.

[30] Y. Ikezoe, N. Hirota, J. Nakagawa, K. Kitazawa, *Nature* **1998**, *393*, 749.

[31] N. Hirota, M. Kurashige, M. Iwasaka, M. Ikehata, H. Uetake, T. Takayama, H. Nakamura, Y. Ikezoe, S. Ueno, K. Kitazawa, *Phys. B Condens. Matter* **2004**, *346-347*, 267.

[32] Y. Ueda, F. Mishima, Y. Akiyama, S. Nishijima, *IEEE Trans. Appl. Supercond.* **2014**, *24*, 1.

[33] G. W. Ehrenstein, *Polymeric Materials: Structure, Properties, Applications*, Hanser Publishers, **2001**.

[34] P. . Thanki, C. Ramesh, R. . Singh, *Polymer (Guildf).* **2001**, *42*, 535.

[35] Tristar, "Rulon Bearings: How to Recognize Genuine and Avoid Counterfeit," **2014**.

Supporting Information for:

Using Magnetic Levitation for Non-Destructive Quality Control of Plastic Parts

Jonathan W. Hennek[1], Alex Nemiroski[1], Anand Bala Subramaniam[1], David K. Bwambok[1], Dian Yang[2], Daniel V. Harburg[1], Simon Tricard[1], Audrey K. Ellerbee[1], and George M. Whitesides[1,3,4,*]

[1]Department of Chemistry and Chemical Biology, Harvard University,

12 Oxford St., Cambridge, MA 02138

[2]School of Engineering and Applied Sciences, Harvard University, 29 Oxford St., Cambridge, MA 02138

[3]Wyss Institute for Biologically Inspired Engineering, Harvard University,

60 Oxford St., Cambridge, MA 02138

[4]Kavli Institute for Bionano Science & Technology, Harvard University, 29 Oxford Street

Cambridge, MA 02138

Orientation of a heterogeneous object with cylindrical symmetry

We have previously shown that the height h and angle of orientation θ of an object in a linear magnetic gradient, and under the influence of gravity, are independent.[12] As such, to study the orientation of the object, we need only consider the angle-dependent part of the potential energy $U(\theta)$, which can be decomposed into a magnetic contribution $U_{mag}(\theta)$, and gravitational contribution $U_{grav}(\theta)$. As we have previously shown[12], in general, U_{mag} will depend on a competition between the lengths of the principal axes $(\lambda_u, \lambda_v, \lambda_w)$ of the object, where (u, v, w) are the body-fixed coordinates in the principal frame of reference of the object. Equation S1 defines the lengths of the principal axes $\lambda_l \in (\lambda_u, \lambda_v, \lambda_w)$ of the object in the body-fixed, principal frame of reference $(\hat{\mathbf{u}}, \hat{\mathbf{v}}, \hat{\mathbf{w}})$; we discuss these values in more depth in Subramaniam *et al*.[12]

$$\lambda_l{}^2 = \frac{\int_V \Delta\chi(l, v, w)\, l^2 dV}{\int_V \Delta\chi(l, v, w) dV} \tag{S1}$$

In general, the λ_l values determine the "size" of the object as seen by the magnetic field, and are therefore determined not just by its geometry of the object, but by the volume distribution of the relative magnetic susceptibility, $\Delta\chi$, as well. In this paper, however, we assume that differences in χ have a negligible effect on the orientation, and thus we assume that it is homogenous throughout the object, in which case the lengths of the principal axes are reduced to Equation S2.

$$\lambda_l{}^2 = \frac{1}{V}\int_V l^2 dV \tag{S1}$$

Here, the origin of a body-fixed principal frame of reference lies at the geometric center (centroid) of the object. For many common parts (such as a screw, washer, or rod with a square cross-section) the lengths of two principal axes of these moments will be degenerate. In this case, without loss of generality, we set $\lambda_u = \lambda_v$, and define the w-axis as the axis of rotational

symmetry of the object. For a rectangular rod with a square cross-section with side width W and length L, the volume is $V = W^2L$, the lengths of the principal axes are given in Eq. S1–S2.

$$\begin{aligned}\lambda_u{}^2 = \lambda_v{}^2 &= \frac{1}{V}\int_V w^2 dV = \frac{1}{W^2L}\int_{-W/2}^{W/2} u^2 du \int_{-W/2}^{W/2} dv \int_{-L/2}^{L/2} dw \\ &= \frac{1}{12} W^2 \end{aligned} \tag{S1}$$

$$\begin{aligned}\lambda_w{}^2 &= \frac{1}{V}\int_V w^2 dV = \frac{1}{W^2L}\int_{-W/2}^{W/2} du \int_{-W/2}^{W/2} dv \int_{-L/2}^{L/2} w^2 dw \\ &= \frac{1}{12} L^2 \end{aligned} \tag{S2}$$

Using the assumptions above, Equation S3 shows $U_{mag}(\theta)$ parameterized by the angle θ between the body-fixed w-axis and the MagLev x-axis.

$$\begin{aligned} U_{mag}(\theta) &= -\frac{2{B_0}^2\Delta\chi}{\mu_o d^2} V\left(\lambda_v{}^2 - \lambda_w{}^2\right)\sin^2\theta \\ &= -\frac{{B_0}^2\Delta\chi}{6\mu_o d^2} V(W^2 - L^2)\sin^2\theta \end{aligned} \tag{S3}$$

In this equation, V is the volume of the object. In the absence of any heterogeneity in density, $U_{mag}(\theta)$ is the only term that contributes a torque about the centroid of the object. For shapes with $W > L$ (e.g. washer), stable orientations occur at $\theta = 0°$ and $180°$. For shapes with $W < L$ (e.g. rod, screw), stable orientations occur at $\theta = 90°$ and $270°$. In general, the object orients to move as much of its volume away from the magnets.

For an object with heterogeneity in density $\rho_s(\vec{r}')$, the center of mass and centroid are not, in general, located at the same point. In these cases, gravity will impart an additional force on the center of mass of the object. The gravitational potential energy $U_{grav}(\theta)$ is defined in Equation S4.

$$U_{grav}(\theta) = -\overline{\rho}_s V g \mathbf{r}_{cm}{}' \cdot \hat{\mathbf{z}}' \tag{S4}$$

In this equation, $\overline{\rho}_s = \frac{1}{V}\int_V \rho_s(\vec{r}')dV$ is the volume-averaged density of the object, g is the acceleration due to gravity, $\mathbf{r}_{cm}{}'$ is location of the center of mass defined in the principal frame, and $\hat{\mathbf{z}}'$ is $\hat{\mathbf{z}}$ parameterized in the principal frame. For an arbitrary $\rho_s(\vec{r}')$, the coordinates of the $\vec{r}_{cm}{}'$ can be found by Equation (S5).

$$\vec{r}_{cm}{}' = \frac{1}{\overline{\rho}_s V}\int_V \vec{r}'\rho(\vec{r}')\, dV \tag{S5}$$

We consider a simple case where defects occur along the principal w-axis such that $\vec{r}_{cm}{}' = (0, 0, w_{cm})$. In particular, we define a small cubic inclusion with density ρ_i, side length l, volume $V_i = l^3$, and displacement z_i along the w-axis of a rod of density ρ_r. In this case, the center for mass is

$$\begin{aligned} w_{cm} &= \frac{1}{\overline{\rho}_s V}\left[\int_{V_r} w\rho_r\, dV - \int_{V_i} w\rho_r\, dV + \int_{V_i} w\rho_i\, dV\right] \\ &= \frac{1}{\overline{\rho}_s V}\left[\rho_r W^2 \int_{-\frac{L}{2}}^{\frac{L}{2}} w dw - \rho_r l^2 \int_{z_i-\frac{l}{2}}^{z_i+\frac{l}{2}} w dw + \rho_i l^2 \int_{z_i-\frac{l}{2}}^{z_i+\frac{l}{2}} w dw\right] \end{aligned} \tag{S5}$$

In the body-fixed frame of reference, $\hat{\mathbf{z}}' = (0, \sin\theta, \cos\theta)$, and therefore $\mathbf{r}'_{cm} \cdot \hat{\mathbf{z}}' = w_{cm}\cos\theta$ and $U_{grav}(\theta) = -\overline{\rho}_s V g\, w_{cm}\cos\theta$. After substituting Equation S5 for w_{cm}, Equation S6 shows the total potential energy of the object in MagLev.

$$U(\theta) = -\frac{{B_0}^2 \Delta\chi}{6\mu_o d^2} V(W^2 - L^2)\sin^2\theta\ - (\rho_i - \rho_r)V_i z_i\ \cos\theta \tag{S6}$$

For the calculations shown in Figure 3, we use the magnetic field B_0 = 0.385 T measured at the surface of the pair of 2" x 2" x 4" magnets separated by d = 4.5 cm. For the rod with L = 2.5 cm and W = 1 cm, we have $V = W^2 L = 2.5$ cm^3 and $W^2 - L^2 = -5.25$ cm^2. In Figure 3,

we find the equilibrium orientation by minimizing $U(\theta)$ with respect to θ for a range of V_i, z_i, and $\Delta\chi$.

To get an intuitive sense of the behavior of objects in this potential well, we normalize the coefficients and extract a general form of the potential energy $U(\theta) = -[\sin^2\theta + A\ \cos\theta]$. In the main text, we measure the angle of inclination $\alpha = 90^\circ - \theta$ from the y-axis (for experimental simplicity); making the substitution we arrive at $U(\alpha) = -[\cos^2\alpha + A\ \sin\alpha]$. In Figure S1, we show how the minimum value of $U(\alpha)$ changes with the relative strength of the magnetic and gravitational contributions (changing value of A).

Use of Rectangular Magnets

For a square magnet and objects that are small relative to the length of the magnet, the object will be free to rotate around the z-axis because of the approximately cylindrically symmetric magnetic field near the z-axis. This random rotation can complicate experimental measurements. To simplify measurements and analysis, we used rectangular magnets and oriented them with the narrower dimension along the x-axis and the wider dimension along the y-axis. Using this configuration increased the magnetic confinement along the x-axis and decreased the confinement along the y-axis (relative to square magnets), thereby breaking the cylindrical symmetry of the magnetic field and constraining the w-axis of the rods to lie in the y-z plane. Furthermore, because ${B_y}^2 \ll {B_z}^2$ in this configuration, the contribution to the energy from B_y can be ignored: in our model, we only consider the effect of B_z.

Figure S1. Plot of $U(\alpha)$ for various values of A. The red arrows show the minimum value α_{min}, where the object will attain a stable equilibrium for each given A. (Inset) Plot of the calculated α_{min} vs. A.

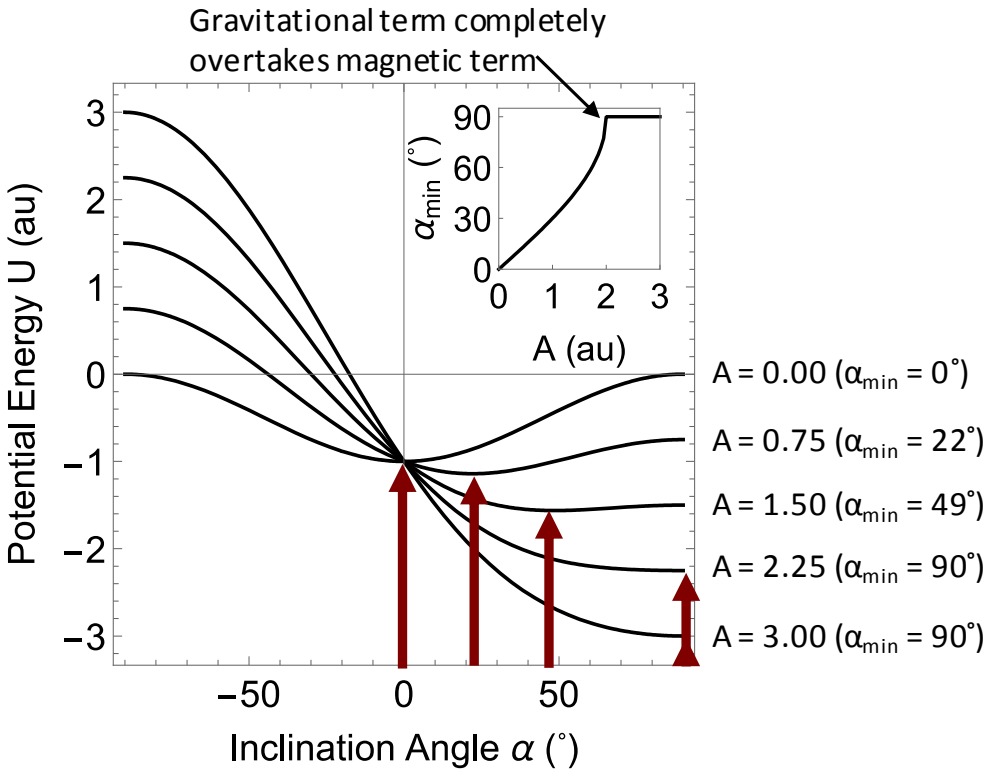

Micro-CT Analysis of Nylon Washers

Micro-CT analysis was performed using a X-Tek HMXST225 tomography system with x-ray voltage and current set to 70 kV and 102 μA, respectively. Data were analyzed using the VGStudio MAX software suite using following steps: 1) surface determination was performed on the objects with "remove small particles and voids" selected (note: if this step was not selected, the subsequent steps required ~40 hours of computation time), 2) a region of interest was selected to remove the sample holder and surrounding air, and 3) defect detection was performed using the porosity/inclusion module (probability threshold > 1, minimum volume = 8 voxel, maximum volume = 5 mm^3). Resulting images were modified using Adobe Photoshop to improve the contrast between the plastic parts and the small colored defects.

3D-Printed Model Rods

Model rods were printed using a Stratasys Objet30 Pro desktop three-dimensional (3D) printer based on drawings produced with Solidworks computer aided design software. The body of the rods was composed of Objet Veroblue RGD 840, a polyacrylate, and inclusions were made from printer support material, a polyacrylate with a lower degree of cross-linking. The density of a pristine rod and an inclusion were determined by levitating the object in 1.0 M $MnCl_2$ in the MagLev configuration described in the main text, measuring the height of levitation, and comparing the height to standards of known density (American Density Materials, Inc.). A linear magnetic field gradient was assumed.

Figure S2. Modeled levitation angle α for polyacrylate rods having ρ = 1.184 g/cm^3 containing a single void (air, ρ = 0.001 g/cm^3) of different volumes. Values are calculated for the same experimental conditions as used in Figure 3a (void = 10 mm from centroid, [$MnCl_2$] = 0.05 M). The largest inclusion volume is only 0.06% of the total volume of the 2.5 x 1 x 1 cm rod. The sensitivity of MagLev is, therefore, quite high when the Δρ between the majority material and the defect is high.

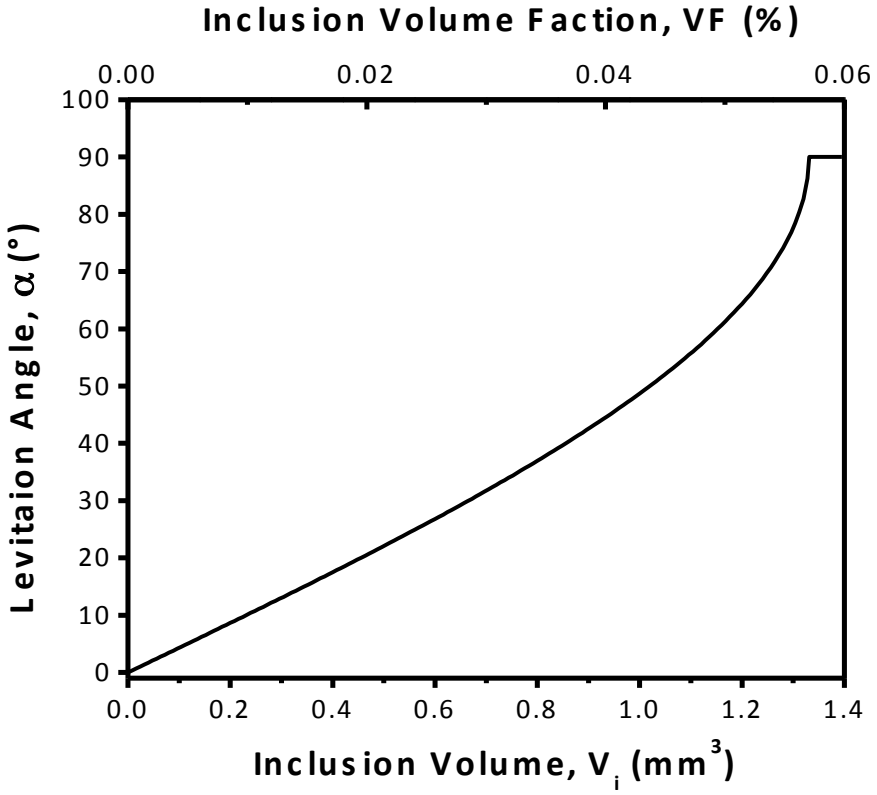

Exposure of Nylon 6/6 Objects to Simulated Harsh Environmental Conditions

We selected seven 3-cm Nylon 6/6 rods, exposed half of each rod to UV light (100 W), and measured α of the rods at 12-hour intervals for 72 hours. Figure S3 shows the α of the rods versus illumination time when levitating in an aqueous solution containing 0.075 M $MnCl_2$ + 1.26 M $ZnCl_2$. At t = 0, a negative α was observed in some cases because the portion of the rod exposed to UV light was chosen at random and α was measured as a deviation above the horizon for the exposed side.

We exposed half of several 3-cm Nylon 6/6 rods to deionized water, sea water (0.60 M NaCl), and a dilute acidic solution (0.10 M HCl) all at 50 °C for 24 hours to characterize the ability of MagLev to detect structural changes in plastic parts after exposure to harsh environments. Rods were placed in an aqueous solution of 0.10 M $MnCl_2$ + 1.26 M $ZnCl_2$ and levitated in a MagLev device (Figure S4). In all cases the exposure to degrading environments leads to a decrease in density of the exposed region.

We mimicked local thermal stress on an object by placing a small metal nut onto the end of a Nylon 6/6 screw and then putting the thermally conductive metal in contact with a hotplate set to 150 °C for 30 minutes. While thermal degradation of Nylon 6/6 typically results in a yellow discoloration, the small area of the exposed region made any potential discoloration undetectable by eye. The screws were then submerged in aqueous solutions of 0.10 M $MnCl_2$ + 1.26 M $ZnCl_2$, placed into the MagLev device, and photographed (Figure S5). The screw tilt angle with respect to the bottom magnet face was measured using ImageJ. As shown in Figure S5, thermal stress decreases the density of Nylon 6/6. The local change in density is detectable by MagLev as seen by an orientation deviation from horizontal.

Figure S3. Levitation angle, α, as a function of time for 3 cm Nylon 6/6 rods after half of the rod was exposed to a 100 Watt UV-light for a total of 72 hours (n = 7). Rods were levitated in an aqueous solution containing 0.075 M $MnCl_2$ + 1.26 M $ZnCl_2$.

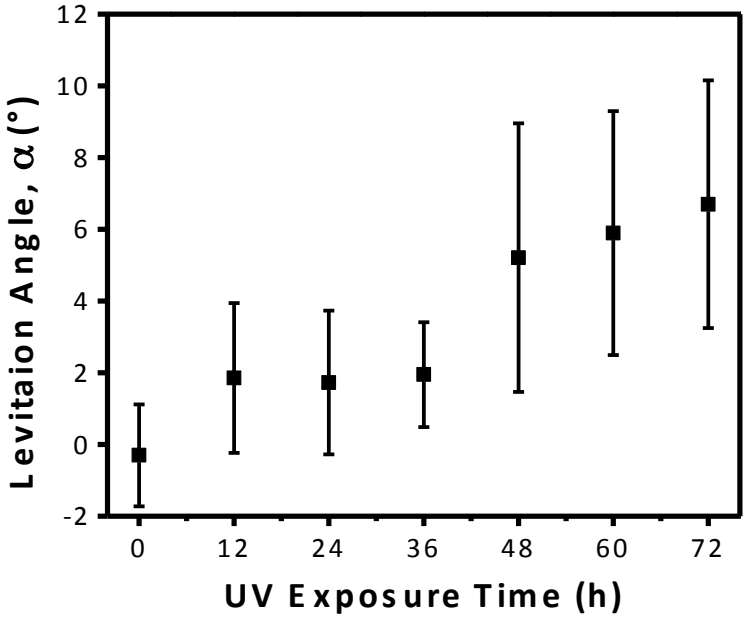

Figure S4. Photographs of Nylon 6/6 rods half of which were exposed to a variety of environmental conditions known to degrade the physical properties of plastics levitating in an aqueous solution of 0.10 M $MnCl_2$ + 1.26 M $ZnCl_2$. Rods were exposed to various degrading environmental conditions at 50 °C for 24 hours. The use of rectangular prism magnets (2.5 x 2.5 x 10 cm) confines the rods along the y-z plane. The pristine rod levitates horizontally to the face of the magnet while the other rods levitate with a deviation ranging from 10-15°, depending on the conditions. In all cases, exposure to degrading environments leads to a decrease in the density of the exposed region. The exposed area is the left half of the rods in the photographs.

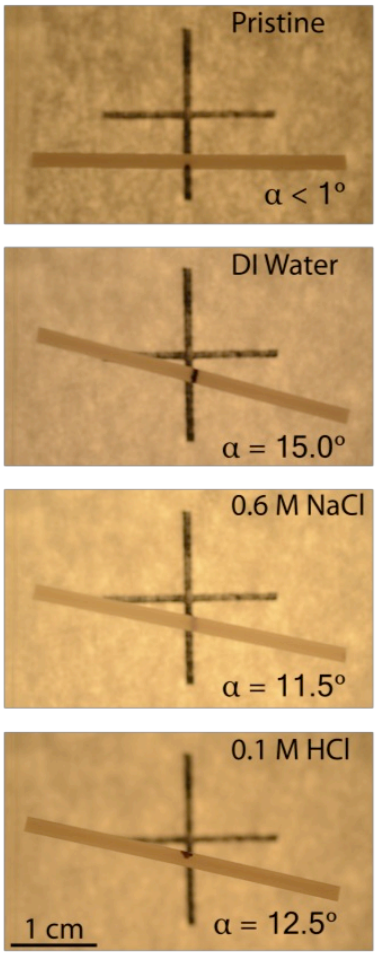

Figure S5. Photographs showing Nylon 6/6 screws levitating in an aqueous solution of 0.10 M $MnCl_2$ + 1.20 M $ZnCl_2$ with rectangular prism magnets (2.5 x 2.5 x 10 cm) placed 5.5 cm apart. A pristine screw (A) levitates with a tilt angle relative to the bottom magnet face of 0°. When screws were subjected to local thermal stress in the highlighted area for 30 minutes at 150 °C, a reduction in density in the affected area causes the screw to tilt with the lower density portion oriented upwards.

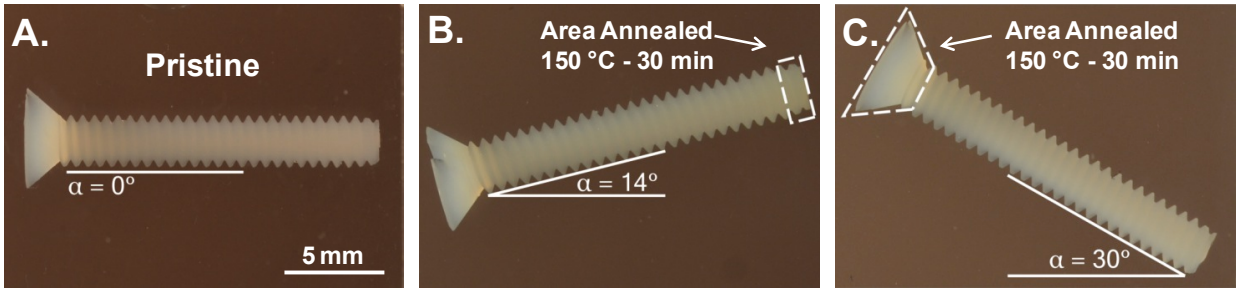

Counterfeit Rulon Detection

We tested real and fake Rulon® J using the same method as described for Rulon® 641. The paramagnetic solution used was 0.24 M $MnCl_2$ in 48% water, 52% Heavy Liquid (GEOLiquids Inc.) having a density of 1.9776 g/cm^3. Seven real and fake sleeve bearings were levitated at the same time and their heights were recorded. Figure S6 shows a box plot of the levitation height of each type. We found for real Rulon® J an $h_{avg} = 2.60 \pm 0.68$ cm ($\rho_{avg} = 1.97 \pm 0.01$ g/cm^3) and for fake Rulon® J an $h_{avg} = 1.16 \pm 0.44$ cm ($\rho_{avg} = 1.99 \pm 0.01$ g/cm^3) corresponding to a p-value of 7.24×10^{-4}.

We also tested Rulon® LR and found that real Rulon® LR is slightly magnetic (presumably ferromagnetic, as a result of metal oxide additives). When the paramagnetic solution was matched to approximately the density of the Rulon® LR bearing and placed in a MagLev device, the bearing was attracted to either the top or the bottom magnet. We found the magnetism of Rulon® LR to be small; a NdFeB magnet with a surface field of 0.4 T is not strong enough to attract the part in air. The fake Rulon® LR samples we tested, on the other hand, were not magnetic and levitated in a 0.50 M $MnCl_2$ (in 30/70 water/Heavy Liquid). Images of real and fake Rulon® LR are shown in Figure S7.

Figure S6. Box plot showing levitation height for real and fake Rulon® J (n = 7) levitating at the same time in 0.24 M $MnCl_2$ 48:52 water:Heavy Liquid mixture.

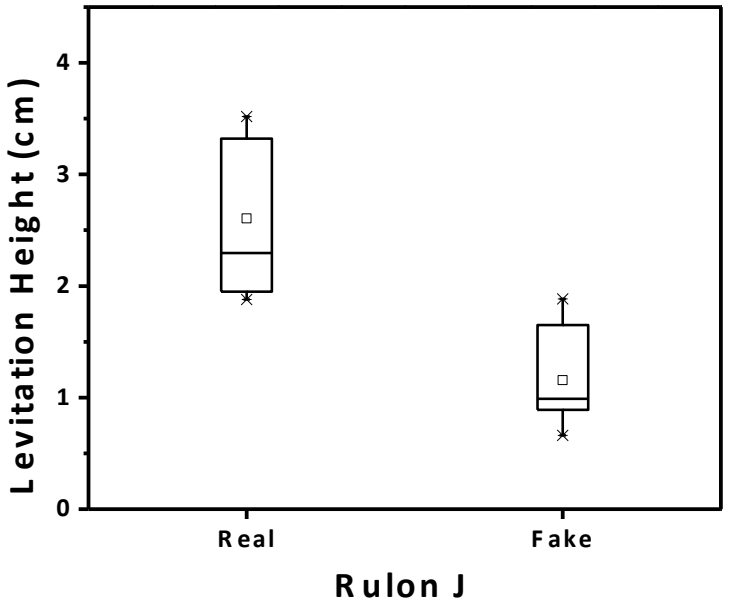

Figure S7. Images of stable levitation positions of real and fake Rulon® LR. The fake Rulon® consistently levitates at ~2.0 cm whereas the real Rulon® LR is attracted to either the top or bottom magnet and does not levitate in the solution. Images are cropped and put side by side for clarity.